

Do High-Frequency Eddies Contribute to Low-Frequency Teleconnection Tendencies?*

PANOS J. ATHANASIADIS

Department of Atmospheric Sciences, University of Washington, Seattle, Washington

MAARTEN H. P. AMBAUM

Department of Meteorology, University of Reading, Reading, United Kingdom

(Manuscript received 24 March 2009, in final form 6 July 2009)

ABSTRACT

An isentropic potential vorticity (PV) budget analysis is employed to examine the role of synoptic transients, advection, and nonconservative processes as forcings for the evolution of the low-frequency PV anomalies locally and those associated with the North Atlantic Oscillation (NAO) and the Pacific–North American (PNA) pattern. Specifically, the rate of change of the low-frequency PV is expressed as a sum of tendencies due to divergence of eddy transport, advection by the low-frequency flow (hereafter referred to as advection), and the residual nonconservative processes. The balance between the variances and covariances of these terms is illustrated using a novel vector representation.

It is shown that for most locations, as well as for the PNA pattern, the PV variability is dominantly driven by advection. The eddy forcing explains a small amount of the tendency variance. For the NAO, the role of synoptic eddy fluxes is found to be stronger, explaining on average 15% of the NAO tendency variance. Previous studies have not assessed quantitatively how the various forcings balance the tendency. Thus, such studies may have overestimated the role of eddy fluxes for the evolution of teleconnections by examining, for example, composites and regressions that indicate maintenance, rather than evolution driven by the eddies. The authors confirm this contrasting view by showing that during persistent blocking (negative NAO) episodes the eddy driving is relatively stronger.

1. Introduction

In the analysis of Athanasiadis and Ambaum (2009, hereafter AA09) it was argued that, if synoptic transients play a role in the existence and the particular characteristics of extratropical teleconnections, this has to be through nonlinear mechanisms, such as the possible forcing of slow anomalies by systematic eddy fluxes. Here we present a potential vorticity analysis of the tendencies of slow (beyond 10 days) anomalies with the aim of identifying the role of the eddy fluxes in the dynamics. More explicitly, we examine the eddy contri-

bution to slow tendencies and not their contribution to the maintenance of slow anomalies. While the latter approach is implicit in most previous studies, the former is arguably more relevant as persistent anomalies represent only a small part of the low-frequency flow.

The studies of Feldstein and Lee (1998), Limpasuvan and Hartmann (2000), and Vallis et al. (2004), each from a different viewpoint, support the idea that the eddy forcing by synoptic-scale transients is important for the maintenance of low-frequency anomalies associated with particular patterns of variability. This forcing has also been examined in a number of other studies following a variety of approaches, from diagnostic to purely theoretical or modeling ones. For example, Branstator (1992) performed a linear, diagnostic model analysis of prominent low-frequency patterns (upper-tropospheric streamfunction EOFs) to distinguish between a number of forcing mechanisms. In the spirit of the linear decomposition of Valdes and Hoskins (1989), Branstator partitioned the total forcing into additive components,

* Joint Institute for the Study of the Atmosphere and Ocean Contribution Number 1759.

Corresponding author address: Dr. Panos J. Athanasiadis, Dept. of Atmospheric Sciences, University of Washington, Box 351640, Seattle, WA 98195-1640.
E-mail: panos@atmos.washington.edu

including the transient eddy fluxes and the interaction between low-frequency anomalies and the climatological stationary eddies. Assessing the role of these forcing mechanisms in a general circulation model simulation, Branstator concluded that the low-frequency anomalies associated with the aforementioned EOFs were primarily maintained by anomalous transient eddy fluxes, with synoptic-scale transients in particular accounting for most of the related response. It is noted, though, that the temporal and spatial variations of the eddy fluxes themselves depend on the low-frequency underlying anomalies, and the described study did not examine how these anomalies become established in the first place.

Robinson (1996, 2000) put forward the idea that synoptic eddies, with their momentum fluxes and in combination with the action of surface drag over time, tend to enhance the westerly flow aloft as well as the local baroclinicity upon which these eddies grow. Following his line of argument, the eddy activity along the mid-latitude jets is thought to exert a positive feedback onto the jets. In his modeling study, Robinson proposes that this mechanism may drive low-frequency zonal index variability in the real atmosphere.

Zonal index variability has also been studied, among others, by Hartmann and Lo (1998), Limpasuvan and Hartmann (2000), and Lorenz and Hartmann (2003). Limpasuvan and Hartmann analyzed data from both a general circulation model and the National Centers for Environmental Prediction–National Center for Atmospheric Research (NCEP–NCAR) reanalysis and found essentially the same hemispheric variability patterns. For the Northern Hemisphere they found that eddy forcing by high-frequency transients projects constructively onto the Northern Annular Mode (NAM) anomalies. In a similar context, Lorenz and Hartmann confirmed this result and further suggested that a feedback interaction occurs between the midlatitude zonal flow anomalies and the synoptic eddy activity, giving rise to zonal index variability. Limpasuvan and Hartmann took composites of the eddy forcing on the NAM index time series and found that the eddy forcing tends to reinforce the concurrent anomalies. Yet, this does not show that the evolution of the anomalies is driven by the eddy forcing. Furthermore, Lorenz and Hartmann computed lag correlations and covariances and found that the synoptic eddy forcing constructively leads the pattern index variability by 1–2 days; however, the significance of this forcing was not assessed in magnitude relative to the pattern (zonal momentum) variability.

Regarding the NAO variability, a different argument has been put forward by Benedict et al. (2004). These authors suggest that it is the wave breaking of synoptic disturbances that generates the individual NAO events.

Examining synoptic maps of potential temperature on the tropopause ($PV = 2$ surface) during a number of strong positive and negative NAO phases, they concluded that successive cyclonic or anticyclonic wave breaking builds and maintains the NAO anomalies correspondingly for the negative or the positive phase. Decay due to mixing is supposed to damp the anomalies after the wave breaking ceases. Given that potential temperature (θ) fluxes on a PV surface are strongly related to PV fluxes on a θ surface, this wave-breaking mechanism seems to require that organized synoptic PV eddy fluxes must occur in the North Atlantic region before the NAO anomalies are formed, as well as during part of their life span.

There is a need to clarify the concept of “eddy driving,” quite apart from the much bigger conceptual difficulties regarding any eddy–mean flow decomposition. Does eddy driving refer to the maintenance of any low-frequency state, or does it refer to the way the low-frequency state is achieved—in other words, to the associated transitions? Although the first interpretation has been implicitly used by most authors, we suggest that the second interpretation may be the more relevant one. While the existence of low-frequency persistent states is still debated, it is clear that these persistent states are not representative of the low-frequency variability of the flow. While the maintenance of low-frequency patterns by eddies has been addressed in various studies, in this study we examine how and to what degree the low-frequency *tendencies* are driven by eddies.

The article is structured as follows. In section 2 we describe the dataset and a spatial filter used in the analysis. We also provide some ordinary diagnostics for the 315-K isentropic surface, which is the level chosen for our analysis. In section 3 we introduce the devised isentropic PV budget method. In section 4 we present results for the point-to-point PV budget evaluation. The same budget for particular patterns of variability is presented illustratively in section 5 by means of a novel vector representation. The PV budget is examined comparatively during a persistent blocking event in section 6 and, finally, section 7 closes with a summary of our findings.

2. Data and the 315-K isentropic surface

To examine the nonlinear interaction between synoptic eddies and various components of the slow-varying, or time-mean, circulation in the troposphere various studies have examined the budget of one or another fundamental variable, such as geopotential height, streamfunction, zonal momentum, quasigeostrophic potential vorticity, etc. For our analysis, given the availability of new datasets, Ertel–Rossby potential vorticity (PV) is chosen among

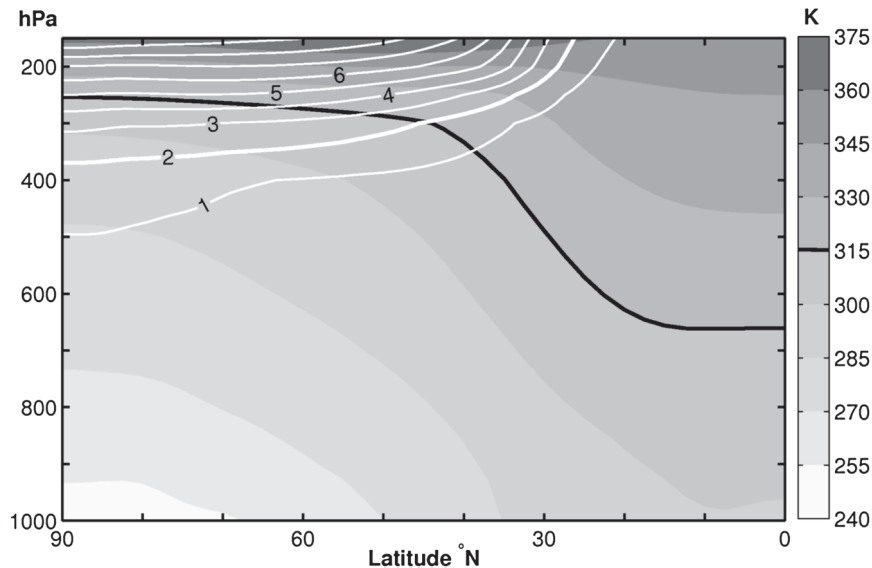


FIG. 1. Pressure–latitude cross section of potential temperature (shading) and potential vorticity (contours) for DJFM. The $PV = 2$ PVU and $\theta = 315$ K contours are highlighted.

other variables as the most meaningful within a dynamical context. Its conservative property allows for a simple budget equation with unambiguous interpretation of the appearing terms. Furthermore, using potential vorticity frees our analysis from the strict assumptions of the quasigeostrophic theory.

The data used in this study consist of daily means of potential vorticity P and horizontal wind components u and v at 315 K from the 40-yr European Centre for Medium-Range Weather Forecasts Re-Analysis (ERA-40; Uppala et al. 2005). These are for the Northern Hemisphere and for the period December–March (DJFM) spanning the years 1957–2002. The data are given on a Gaussian grid with spatial resolution of about $2.25^\circ \times 2.25^\circ$, which corresponds to a spacing of about 250 km. The wind includes the irrotational component. Throughout this study PV is expressed in PV units (PVU), where $1 \text{ PVU} \equiv 10^{-6} \text{ km}^2 \text{ kg}^{-1} \text{ s}^{-1}$.

The isentropic surface 315 K was chosen for the analysis as the one that, during the Northern Hemisphere winter, lies the most in the troposphere without intersecting the ground, except at the Himalayas. In Fig. 1, it is seen that, in the zonal-mean winter climatology, this isentrope slopes from about 250 hPa at the North Pole to approximately 650 hPa at the equator, intersecting the dynamical tropopause $PV = 2$ at $\sim 45^\circ\text{N}$.

Swanson (2001) demonstrates the striking difference between the time mean and the mode of the PV distribution on isentropic surfaces aloft. Characteristically, the mode distribution exhibits a much sharper gradient. The smoother time-mean distribution is the result of the undulating tropopause-crossing line, with high strato-

spheric PV values inside (poleward) and considerably lower tropospheric values outside (equatorward). This undulating motion integrated in time widens the steep instantaneous meridional PV gradient. The wavenumber 2 distribution of the time mean is characteristic of the Northern Hemisphere winter stationary waves. After removing the zonal mean, Derome et al. (2001) find the climatological positive zonal PV anomalies to be on the poleward side of the North Pacific and North Atlantic storm track entrances and the associated jet maxima, where the strongest cyclonic wind shear is also located.

Figure 2 displays the PV variance for daily time series and the contribution to this variance by the high-frequency and the low-frequency transients. It is worth noticing that the high-frequency band ($T < 10$ days) contains approximately half of the total daily variance, while for sea level pressure and geopotential height at midtroposphere the corresponding percentage is approximately a quarter of the total, as documented in AA09. Not surprisingly, the synoptic-scale transients in Fig. 2b show maximum variability at the same locations where storm activity takes its maxima, as indicated by upward heat flux at 700 hPa or by transient eddy kinetic energy at 250 hPa (Kållberg et al. 2005). On the other hand, low-frequency transients show maximum variability farther downstream, close to the exits of the storm tracks where blocking episodes are most frequent (Tyrlis and Hoskins 2008).

For graphical presentation or for reliable calculation of the spatial derivatives, a scale-selective filter is applied based on Fourier transforms along latitude cycles and half meridians (equator–North Pole–equator) with the vanishing PV and weak wind in the tropics serving

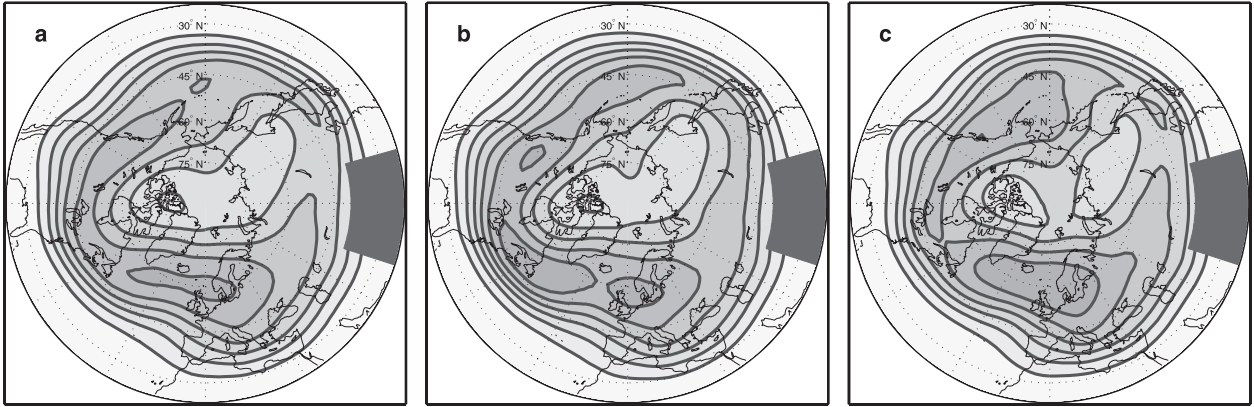


FIG. 2. (a) Variance of PV daily means at $\theta = 315$ K for DJFM, contour interval 0.6 PVU^2 . Variance for the (b) high-frequency and (c) low-frequency transients, contour interval 0.3 PVU^2 . The frequency bands are defined in section 3. Due to orthogonality, (a) = (b) + (c). An extended area around the Himalayas is masked since the data are ill-defined there due to intersection with the ground.

as an approximate periodic boundary condition. Each coefficient of the transformed field along a given line is multiplied with the exponential, $\exp(-k^2/k_o^2)$, where k is the corresponding wavenumber and $k_o = 2\pi/L_o$. An analogous filter for spherical harmonics has been introduced by Sardeshmukh and Hoskins (1984). The length scale L_o is chosen according to the need; that is, to smooth derivatives so as to make sure that errors due to discretization are kept small in calculating eddy fluxes, a synoptic wavelength of $L_o = 1000$ km has been used. The derivatives are easily obtained by applying a $\pi/2$ phase shift to all harmonics before the inverse Fourier transform. Instead, when the filter is used to smooth fields, prior to plotting for better demonstration, $L_o = 1500$ km was found to work best, giving sufficient smoothing without losing the meaningful details.

3. Introduction of the PV budget approach

The present analysis is based on the isentropic PV equation (e.g., in Holton 2004):

$$\frac{\partial P}{\partial t} + \mathbf{v} \cdot \nabla P = -\dot{\theta} \frac{\partial P}{\partial \theta} + P \frac{\partial \dot{\theta}}{\partial \theta} + \frac{1}{\sigma_\theta} \mathbf{k} \cdot \left(\frac{\partial \mathbf{v}}{\partial \theta} \times \nabla \dot{\theta} + \nabla \times \mathbf{F} \right) \equiv \mathcal{R}. \quad (1)$$

For examining the PV balance and the evolution of the low-frequency anomalies our approach goes as follows. First, a cutoff frequency f_c is defined as the limit between *low* and *high* frequencies. Then the quantities appearing in Eq. (1) are partitioned into the corresponding low- and high-frequency components using the same Fourier filtering as described in AA09, giving $X = \bar{X} + X'$, with $\bar{X}' = 0$, due to the orthogonality of Fourier components. The overbar denotes the low-frequency component, which

contains the time mean. Applying the corresponding low-pass filter to the equation leads to

$$\frac{\partial \bar{P}}{\partial t} \equiv \bar{\mathcal{T}} = \bar{\mathcal{A}} + \bar{\mathcal{E}} + \bar{\mathcal{R}}, \quad (2)$$

where

$$\bar{\mathcal{A}} = -\bar{\nabla} \cdot \bar{\nabla P}, \quad (3)$$

$$\bar{\mathcal{E}} = -\bar{\nabla} \cdot \bar{\nabla P}' - \bar{\mathbf{v}}' \cdot \bar{\nabla P} - \bar{\mathbf{v}}' \cdot \bar{\nabla P}', \quad (4)$$

and

$$\bar{\mathcal{R}} = \bar{\mathcal{R}}. \quad (5)$$

Equation (2) expresses the evolution of the low-frequency PV anomaly. The left-hand side tendency $\bar{\mathcal{T}}$ is equilibrated by the right-hand side forcing terms, hereafter referred to as advection $\bar{\mathcal{A}}$, eddy $\bar{\mathcal{E}}$, and residual $\bar{\mathcal{R}}$. This equation holds as a local instantaneous balance.

At this point it should be emphasized that the cross-frequency terms in Eq. (4), such as $\bar{\mathbf{v}}' \cdot \bar{\nabla P}$, are not necessarily zero as they would be if the overbar denoted time averaging. To show this with an example, one can consider the product below [Eq. (6)], where $\omega_1 < 2\pi f_c < \omega_2$. As the right-hand side indicates, depending on the frequencies of the particular Fourier components, a cross-band product may have components in both frequency bands:

$$2 \cos(\omega_1 t) \cos(\omega_2 t) = \cos\left(\frac{\omega_1 + \omega_2}{2} t\right) + \cos\left(\frac{\omega_1 - \omega_2}{2} t\right). \quad (6)$$

It is noted, however, that the eddy forcing ($\bar{\mathcal{E}}$) is dominated by the last term on the rhs of Eq. (4). One should also note that the low-frequency components in Eqs. (3)

and (4) include the time mean. Therefore, part of the advection term is due to products of the low-frequency flow with the (locally large) time-mean PV gradient. On the other hand, similar products in the eddy term (high-frequency flow \times time-mean PV gradient) do not survive the subsequent low-pass filtering.

Brunet et al. (1995), Edouard et al. (1997), and Derome et al. (2001) have studied the time-mean PV budget in isentropic coordinates, and the approach described here bears some similarities with their choices of frequency bands and term partitioning. Also, in the analysis of Sheng and Derome (1993), the low-frequency geopotential height tendency is expressed in a way analogous to Eqs. (2)–(4).

To examine the role of the forcing terms, let \mathbb{T} , \mathbb{A} , \mathbb{E} , and \mathbb{R} also denote the corresponding time series. Then, by identity,

$$\text{var}(\mathbb{T}) = \text{cov}(\mathbb{T}, \mathbb{A}) + \text{cov}(\mathbb{T}, \mathbb{E}) + \text{cov}(\mathbb{T}, \mathbb{R}), \quad (7)$$

with $\text{var}(X)$ denoting the variance of X and $\text{cov}(X, Y)$ denoting the covariance of X and Y . This shows how the variability of the tendency \mathbb{T} is balanced by the covarying forcing terms. Analogous equations can be written for the variance of \mathbb{A} and \mathbb{E} (see equation system below).

Of course, the variance of the tendency term \mathbb{T} is something different than the variance of the low-frequency PV anomaly itself. However, note that the focus is on understanding the *evolution* of the PV anomalies. Therefore, a forcing term may drive slow PV anomalies by synchronously inducing (quantitatively balancing) the corresponding tendency, while a strong covariance between \mathbb{T} and \mathbb{A} or \mathbb{E} or \mathbb{R} would indicate an active forcing. Here “strong” is meant relative to the variance of \mathbb{T} .

Another relevant point is that, since the bounding relationship between the time series in Eq. (2) is a four-component equality, the balance between the four terms should be studied as a whole. In other words, trying to understand how these terms are balanced instantaneously at a given location involves the determination of all the covariances between these time series.

Introducing an alternative compact notation, let $\langle X, Y \rangle$ denote the covariance between X and Y , and $\langle X, X \rangle$ be the corresponding variance. Obviously $\langle X, Y \rangle = \langle Y, X \rangle$. Then, a set of four equations analogous to Eq. (7) can be written as

$$\begin{aligned} \langle \mathbb{T}, \mathbb{T} \rangle - \langle \mathbb{T}, \mathbb{A} \rangle - \langle \mathbb{T}, \mathbb{E} \rangle - \langle \mathbb{T}, \mathbb{R} \rangle &= 0 \\ \langle \mathbb{A}, \mathbb{T} \rangle - \langle \mathbb{A}, \mathbb{A} \rangle - \langle \mathbb{A}, \mathbb{E} \rangle - \langle \mathbb{A}, \mathbb{R} \rangle &= 0 \\ \langle \mathbb{E}, \mathbb{T} \rangle - \langle \mathbb{E}, \mathbb{A} \rangle - \langle \mathbb{E}, \mathbb{E} \rangle - \langle \mathbb{E}, \mathbb{R} \rangle &= 0 \\ \langle \mathbb{R}, \mathbb{T} \rangle - \langle \mathbb{R}, \mathbb{A} \rangle - \langle \mathbb{R}, \mathbb{E} \rangle - \langle \mathbb{R}, \mathbb{R} \rangle &= 0. \end{aligned} \quad (8)$$

Considering the four terms involving the residual \mathbb{R} as the unknowns in this linear algebraic system, these are

uniquely determined in terms of the remaining variances and covariances, which are explicitly calculated from the time series of \mathbb{T} , \mathbb{A} , and \mathbb{E} . Incidentally, this is equivalent to calculating the residual term directly from Eq. (2) and from this the corresponding covariances. Finally, the system of equations (8) applies to every grid point.

4. Application of the PV budget analysis

The balances corresponding to the first three equations in (8) are illustrated as a table of plots in Fig. 3. In this table of plots each column expresses the balance for a single term (\mathbb{T} , \mathbb{A} , \mathbb{E}) as given by the corresponding equation. In each column, the top field equals the sum of the fields underneath. These results are for a cutoff frequency: $f_c^{-1} = 10$ days. A mask has been applied to an extended region around the Himalayas where the isentropic surface occasionally intersects the ground. Prior to plotting, the fields have been gently smoothed, as described in section 2. Finally, it should be noted that in Fig. 3 there are pairs of plots (e.g., $\langle T, A \rangle$ and $\langle A, T \rangle$) displaying the same field with different contour intervals so as to facilitate a meaningful display.

In the left column of the plots in Fig. 3 it is seen that the tendency variance is balanced almost exclusively by the covarying advection \mathbb{A} . Compared to the right column, it is seen that the eddy-forcing term (\mathbb{E}) exhibits four times the variance of \mathbb{T} , and its variability is also largely balanced by advection. Finally, the variance of the advection term itself is even larger, and it is balanced mostly by the residual and partly by the eddy term. To summarize, \mathbb{A} , \mathbb{E} , and \mathbb{T} have significantly different variances. Here \mathbb{A} alone balances the variability of both the other two terms, while, itself is balanced by the residual \mathbb{R} and in some locations partly by \mathbb{E} .

Regarding the spatial distribution of these variances and covariances, one can see that, first \mathbb{T} variance is largest over southern Scandinavia and northwestern Canada, similar to the variance of the low-frequency PV in Fig. 2c, and, second, \mathbb{A} variance is maximal over northern Japan and Quebec, locations where the PV gradient shows its maxima (Massacand and Davies 2001) and the wind is strongest. Finally, the \mathbb{E} variance has its maximum over Quebec where strong high-frequency variability (Fig. 2b) is combined with a large PV gradient.

Seeing that the advection and the residual terms dominate the variability in Eq. (2), it is useful to discuss what this residual term may represent. First of all, it is necessary to recognize that apart from its physical meaning as representing nonconservative effects, the residual term also carries any accumulated computational errors made in the calculation of the remaining terms. Such “errors” may arise, for example, due to unresolved spatial and

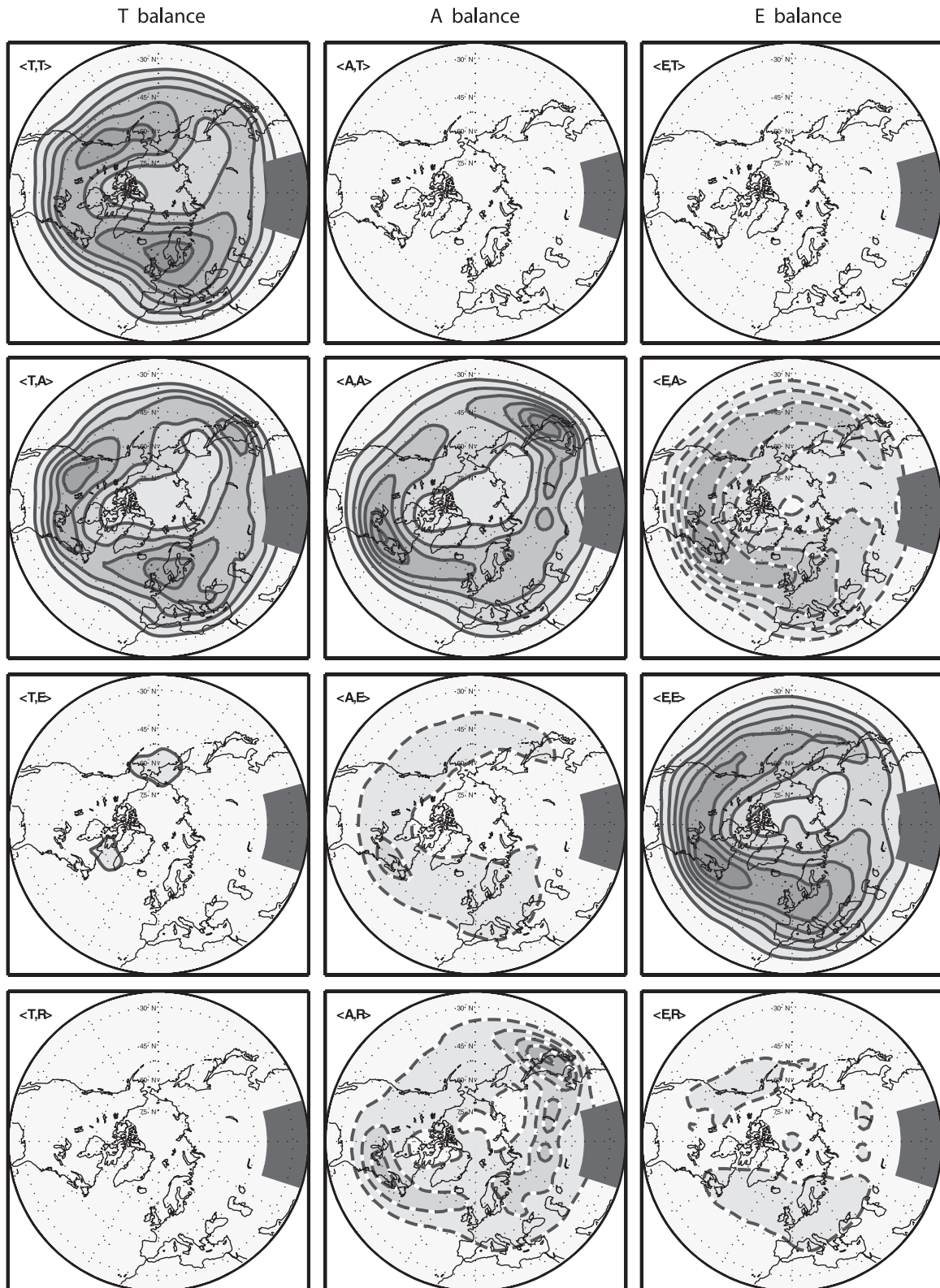


FIG. 3. Each column in the plots illustrates a balance of (co)variances as in Eq. (8). The top field equals the sum of the fields below. Dashed contours are for negative variances. Contour interval (left to right) is 0.025, 0.25, and 0.1; the outermost contour is nearest to the zero contour, which is omitted. Cutoff period is 10 days.

temporal scales. Although, eddy fluxes related to sub-grid and subdaily fluctuations are expected to be small compared to the synoptic eddy fluxes in the free atmosphere, one should remember that the often extremely tight existing PV gradients may be poorly represented by the reanalysis data spatial resolution. Considering now the role of differential diabatic heating, the latter appears to be another likely component represented by \mathbb{R} . Away from the surface, the latent heating related to weather systems arguably dominates the diabatic heating, and therefrom the residual term may in part represent nonconservative effects related to synoptic eddy activity, something that is not included in \mathbb{E} . As follows from the definition of \mathbb{R} , to estimate the net diabatic effects one would have to calculate the term $P(\partial\theta/\partial\theta)$, which dominates the residual at the upper levels according to Hoerling (1992). PV generation by differential latent heating at the upper levels along the storm tracks presumably varies strongly enough as to explain part of the large residual variance. In any case, however, the residual term \mathbb{R} does not project strongly on the tendencies \mathbb{T} , as seen in Fig. 3.

In the limit of very low cutoff frequencies, transients are defined as deviations from the time mean, and the tendency falls to zero. Derome et al. (2001) have examined the time-mean PV budget on the 315-K surface for DJF, partitioning the seasonal anomalies to high- and low-frequency transients with a cutoff period of 10 days and using terms similar to ours. With our own dataset and for DJFM we obtained corresponding results (not shown) comparable to theirs; that is, the mean advection forcing is balanced by the transient eddy forcing or the residual forcing, depending on the location. For the time-mean budget the high-frequency eddy forcing component balances about 50% of the advection forcing at the western North Atlantic and North Pacific.

To see the transition to this type of balance (with zero tendency), the presented analysis was performed also for cutoff periods of 20, 30, and 60 days, approaching the limit where transients are defined as departures from the seasonal mean. To save space, these results are presented in a compact way: the area average of each field is taken from 30°N poleward, and the resulting numbers are tabulated in Table 1 using the same arrangement as in Fig. 3. In the table it can be seen that the \mathbb{T} variance drops roughly proportionally to the squared cutoff frequency. This is understood if one considers that the variance of the low-frequency tendency is dominated by the fastest components with frequencies near the cutoff. On the other hand, the variance of \mathbb{A} and \mathbb{E} show much weaker dependence on the cutoff, which is not surprising given that these are advective terms (velocity \times gradient), and there is no reason for the magnitude of the associated

TABLE 1. Variances (boldface) and covariances for and between the terms \mathbb{T} , \mathbb{A} , \mathbb{E} , and \mathbb{R} averaged from 30°N poleward. Units are 10^{-2} (PVU day $^{-1}$) 2 .

Cutoff period		\mathbb{T}	\mathbb{A}	\mathbb{E}
10 days	\mathbb{T}	7.860	6.558	0.567
	\mathbb{A}	6.558	66.170	-23.503
	\mathbb{E}	0.567	-23.503	31.300
	\mathbb{R}	0.735	-36.109	-7.230
20 days	\mathbb{T}	2.100	1.558	0.314
	\mathbb{A}	1.558	41.560	-18.404
	\mathbb{E}	0.314	-18.404	24.350
	\mathbb{R}	0.248	-21.598	-5.652
30 days	\mathbb{T}	0.820	0.538	0.166
	\mathbb{A}	0.538	31.260	-14.916
	\mathbb{E}	0.166	-14.916	19.720
	\mathbb{R}	0.116	-15.806	-4.638
60 days	\mathbb{T}	0.171	0.103	0.037
	\mathbb{A}	0.103	19.720	-9.724
	\mathbb{E}	0.037	-9.724	13.082
	\mathbb{R}	0.031	-9.897	-3.321

velocities and the PV gradients to vary strongly with f_c . Examining the balance of \mathbb{T} for the different cutoff frequencies, it is seen that the eddy forcing becomes significant for the (decreasing) tendency as the transients include slower and slower components, finally balancing about 20% of the tendency variance in the limit of the longest cutoff period (60 days).

The results presented so far are summarized as follow:

- The low-frequency PV tendency variability is balanced by the advection forcing, indicating that the latter forces the evolution of the associated PV anomalies. The low-frequency PV tendency (as well as the anomalies themselves) shows maximum variance at the exit of the North Pacific and North Atlantic storm tracks where blocking is more frequent.
- The eddy forcing exhibits strong variability (with a maximum over Quebec) but it projects weakly on the slow PV tendency. Instead, its variability is counterbalanced by advection. This indicates that the eddy fluxes are strong but do not in a systematic way contribute to local slow variability. As far as the slow variability is concerned, the eddies, to first order, may be viewed as stochastic forcing.
- For longer cutoff periods the tendency drops and the transient eddies include slower components. Then, it is found that the PV budget tends to a three-term balance—that is, advection \mathbb{A} , eddy forcing \mathbb{E} , and residual forcing \mathbb{R} —with the advection equilibrated by the other two.

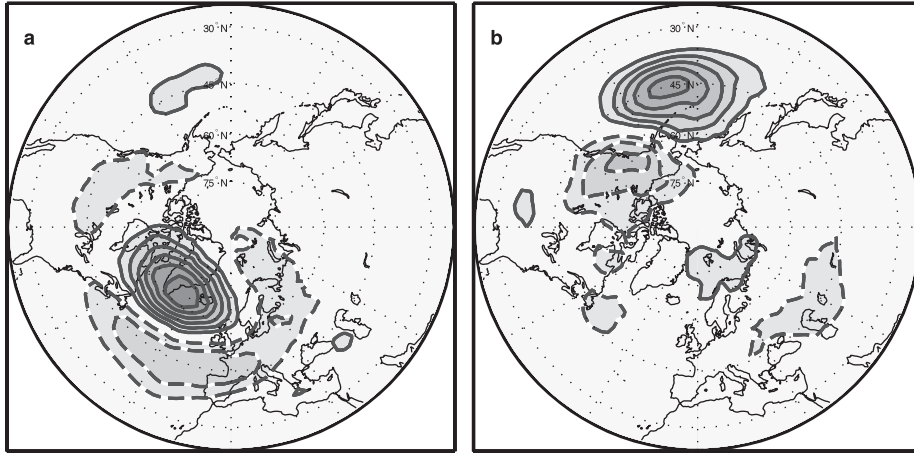


FIG. 4. Regressions of the low-frequency PV tendency field onto the low-frequency tendency of the (a) NAO and (b) PNA daily indices. Cutoff period is 30 days. Contour interval is 1 PVU day⁻¹.

Given the consensus that synoptic eddies are important in driving low-frequency variability in the extratropics—as stated, for example, by Swanson (2002)—the results presented so far may appear somehow unexpected. The dominance of the low-frequency advection forcing for counterbalancing the eddy forcing and driving the low-frequency PV tendency is characteristic in our analysis. This point is discussed further in the closing section.

5. The PV budget for teleconnections

The PV budget analysis in the previous section was performed on a point-to-point basis. However, low-frequency variability follows certain patterns, and in studying their dynamics it is of particular interest to examine how the respective PV anomalies are forced. For this, one needs first to isolate the variability that follows each particular pattern from the bulk of low-frequency variability and then analyze its balance. In this section, following the PV budget approach as in the previous section, the terms \mathbb{T} , \mathbb{A} , \mathbb{E} , and \mathbb{R} (all consisting of a time series at every grid point) are projected onto a nondimensionalized spatial pattern that represents the PV signature of a particular teleconnection, so a single time series is thus obtained for each term. These time series are used to express the PV balance for the examined pattern in terms of the corresponding variances and covariances.

Before studying the PV balances associated with particular teleconnections, the corresponding patterns have first to be defined. For this purpose it was chosen to project the low-frequency PV tendency field (term \mathbb{T}) onto the low-frequency tendency of the NAO and Pacific–North American (PNA) daily indices (cutoff period of 30 days). This choice is justified in the interest of studying the evolution of the PV anomalies rather than the anomalies

themselves. Figure 4 shows the two obtained patterns. The respective time series were standardized prior to performing the projection; thus, the patterns carry the same units as the PV tendency.

Projections of the terms \mathbb{T} , \mathbb{A} , and \mathbb{E} onto the patterns in Fig. 4 are computed taking into account the varying area that grid boxes represent at different latitudes. Assuming \mathbb{T} , \mathbb{A} , and \mathbb{E} are matrices of dimensions $n \times m$, where m represents the number of grid points and n is the length of the time series, and $\mathbf{P}_{m \times 1}$ is a particular pattern, the projection that gives, for example, the time series for the tendency term is performed as follows:

$$\mathbf{T}_i = \frac{1}{\|\mathbf{P}\|} \sum_{j=1}^m \mathbb{T}_{i,j} \mathbf{P}_j \cos \phi_j, \quad \forall i \in \{1, 2, 3 \dots n\}, \quad (9)$$

where $\|\mathbf{P}\|$ is the Euclidean norm of the vector $\mathbf{P}_j \sqrt{\cos \phi_j}$. Equation (9) is the discretized version of the surface integral that defines projection [e.g., Von Storch and Zwiers (1999)]. The resulting time series retain the same dimensions with the original data (i.e., PVU day⁻¹).

As in the previous section, let us use T , A , E , and R to denote the corresponding time series, here representing the variability of the \mathbb{T} , \mathbb{A} , \mathbb{E} , and \mathbb{R} terms projected onto a given pattern. These time series obey the simple instantaneous relationship below, where the subscript is the time index:

$$T_i = A_i + E_i + R_i, \quad (10)$$

For T , A , E , and R a system of equations analogous to Eq. (8) exists, uniquely relating the variances and covariances between the different time series. To depict illustratively how the balance is maintained between the four time series, the variability of each one of them can

be represented by a vector, and thus the temporal covariances between the time series can correspond to the dot products between the four vectors. Precisely, for each time series X , we define a vector \mathbf{X} with a norm equal to the time series standard deviation,

$$\|\mathbf{X}\| = \sqrt{\mathbf{X} \cdot \mathbf{X}} \equiv \sqrt{\langle X, X \rangle}, \quad (11)$$

and the angle between \mathbf{X} and another vector \mathbf{Y} to be defined through

$$\cos\phi_{XY} = \frac{\langle X, Y \rangle}{\sqrt{\langle X, X \rangle \langle Y, Y \rangle}}. \quad (12)$$

The reader will recognize the right-hand side of the equation above as the Pearson correlation coefficient between the time series X and Y . This gives a clear physical meaning to the angle between the respective vectors. From Eqs. (11) and (12) and the definition of the dot product, it follows that

$$\mathbf{X} \cdot \mathbf{Y} \equiv \langle X, Y \rangle. \quad (13)$$

Then, if one positions the corresponding tendency time series vector \mathbf{T} (or any of the \mathbf{A} , \mathbf{E} , or \mathbf{R}) along a particular direction, the remaining vectors take well-defined relative directions. It can be shown that this is a consistent description in terms of the closure of the resulting equations analogous to Eq. (8). In other words, a set of balanced vectors transforms to a uniquely defined set of balanced variances and covariances and vice versa.¹

Using this illustrative representation, Fig. 5 shows the vector balances corresponding to the variances and covariances of the time series $-T, A, E,$ and R as obtained for the NAO and PNA patterns shown in Fig. 4. By definition it follows that

$$\mathbf{T} + \mathbf{A} + \mathbf{E} + \mathbf{R} = 0. \quad (14)$$

The vector diagrams in Fig. 5 are quite similar. A noticeable difference is that for the NAO the eddy-forcing vector \mathbf{E} is longer and less orthogonal to the tendency vector \mathbf{T} (indicating higher correlation), thus requiring a smaller projection of the advection vector \mathbf{A} onto the tendency vector. It is also noted that in both cases the

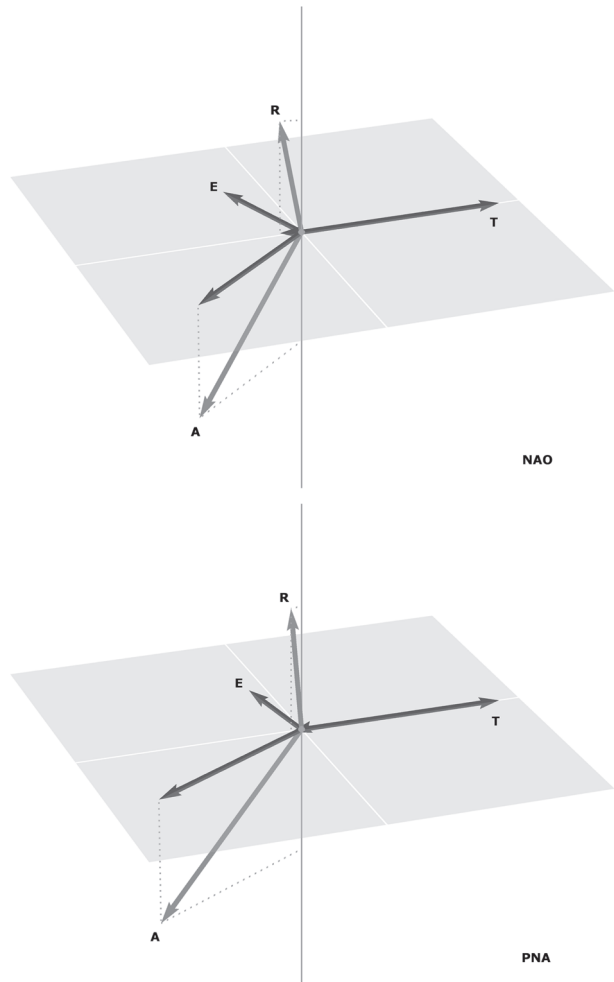


FIG. 5. The norms of the vectors are proportional to the variances of the corresponding time series for a given pattern (Figs. 4a and 4b). The dot products between the vectors are proportional to the corresponding covariances. Relative angles are determined by Eq. (12). Projections of the vectors \mathbf{A} and \mathbf{R} on the (\mathbf{E}, \mathbf{T}) plane are shown. The shaded area represents a rectangle on the (\mathbf{E}, \mathbf{T}) plane. All the vectors are scaled relative to a fixed-length \mathbf{T} vector.

residual forcing vector \mathbf{R} is almost orthogonal to the \mathbf{E}, \mathbf{T} plane. Advection \mathbf{A} has the largest norm (variance) and is fundamental in balancing each of the $\mathbf{T}, \mathbf{E},$ and \mathbf{R} . Given the constraint of Eq. (14), the vectors $\mathbf{T}, \mathbf{E},$ and $(\mathbf{A} + \mathbf{R})$ must lie on the same plane. As seen in the vector balance plots (Fig. 5), each of the vectors \mathbf{T} and \mathbf{E} is largely counterbalanced by $(\mathbf{A} + \mathbf{R})$.

To examine the temporal behavior of these forcings with respect to the NAO life cycle, we show lag statistics in Fig. 6. In particular, the PV tendency (T), advection (A), and eddy forcing (E) projected onto the NAO pattern (Fig. 4) are composed around local maxima and minima of the low-pass filtered daily NAO index, and cross-covariances of the same three terms are taken with the tendency term. All local maxima and minima of the NAO index (referred

¹ Given the variances and covariances, the lengths of the four vectors are defined through Eq. (11). Then, one can place one vector of choice along the Ox semiaxis and another vector on the x - y plane at an angle given by Eq. (12). Any of the remaining two vectors will lay on the intersection of two cones, the opening angles of which are also defined by Eq. (12). Then, the fourth vector can be rightly placed so as to make a balanced tetrad. This leads to more than one symmetric tetrad, but the relative angles between the vectors are always the same.

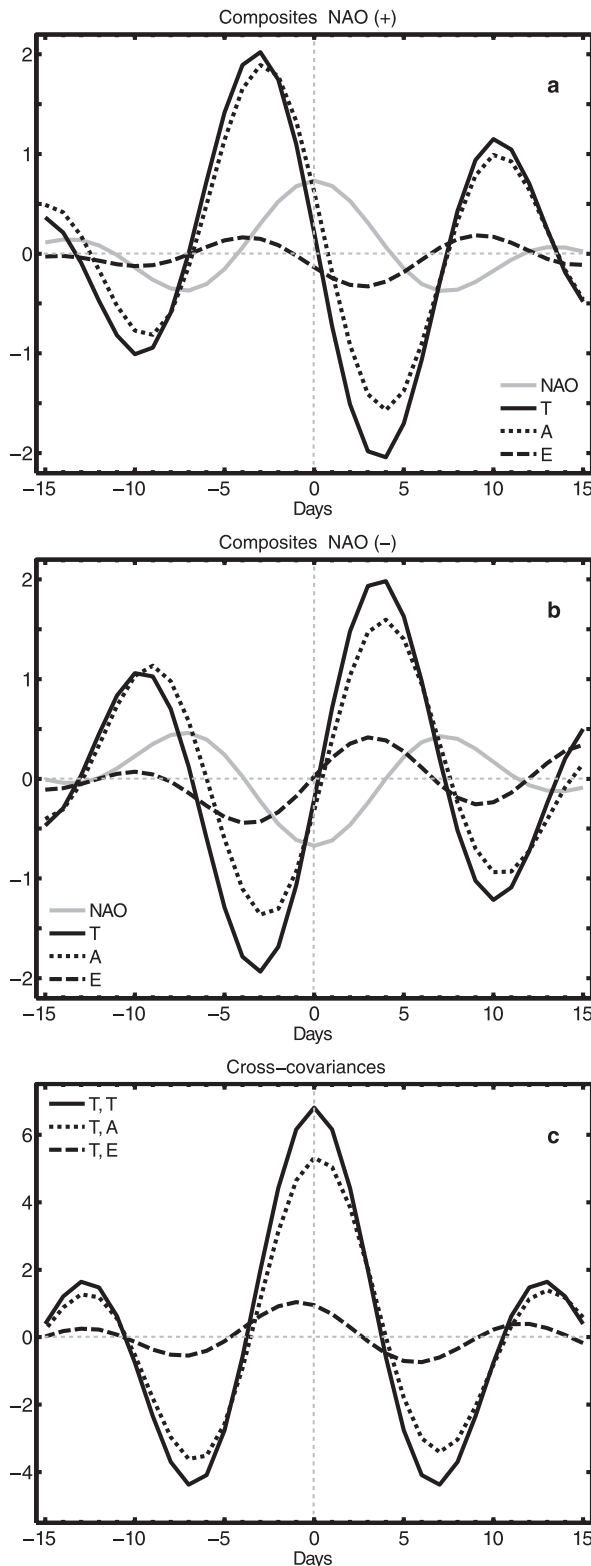


FIG. 6. Lag composites of the tendency (**T**), advection (**A**), and eddy forcing (**E**) around the local (a) maxima and (b) minima of the low-frequency daily NAO index. Units are PVU day^{-1} . (c) Cross-covariances of the same three terms with the tendency. Units are as above but squared.

to as events) are included in the composite analysis without the constraint of any threshold value. Limiting the events with a threshold of one standard deviation for the absolute value of the NAO index (results not shown) did not affect the conclusions drawn from this analysis.

Focusing first on the composites (Figs. 6a and 6b), we see that the tendency crosses the zero line almost at the same time when the NAO index attains its extreme. The tendency is largely driven by the covarying advection. The eddy forcing seems to be slightly ahead of the tendency and to change sign during the NAO cycle, both in the positive and the negative composites. Adding together the advection and eddy forcings yields a good match of the tendency. This is also the case in the plot showing the corresponding cross covariances (Fig. 6c). This confirms that in our analysis the residual term is of little importance for the tendency balance. For lag zero, this is shown in a different way in Fig. 5 by the small projection of **R** onto the (**E**, **T**) plane. It is important to notice that the eddy forcing is largely in phase with the tendency; thus it helps the NAO evolution.

Our result that the eddy forcing changes sign during the NAO life cycle appears to disagree with some previous studies. In particular, Feldstein (2003) performed a composite analysis similar to ours looking into the dynamics of the NAO growth and decay and he found that the eddy forcing [ξ_6 term in his Eq. (1)] remains positive throughout the entire life cycle; namely, it tends to reinforce the pattern anomaly at all times. On the other hand, his term ξ_5 , which corresponds to our advection term, appears to covary with the pattern tendency (rate of change of his $\alpha(t)$ pattern amplitude) in a way similar to our advection term. Note that Feldstein composites around the NAO onset time rather than around the time of the pattern amplitude extreme. This induces an asymmetry around the time of zero tendency (lag + 3 days), which is apparent in his plots. Moreover, the departures between the tendency and the total forcing with the residual neglected (in Feldstein's Fig. 5) look rather significant. Finally, the streamfunction tendency decomposition introduced by Cai and Van Den Dool (1994) and employed in Feldstein (2003) involves some large terms that tend to cancel out. In summary, the apparent inconsistencies appear to be due to the chosen analysis methodology. This does highlight the care that needs to be taken when drawing general conclusions from a single analysis.

As a variant of our method, we also tried applying an additional, final low-pass filter (cutoff period of 20 days or longer) applied to all terms in Eq. (2) before calculating the statistics so as to focus beyond intermediate frequencies (band-2 in AA09), where teleconnections are not clearly prominent. The results of this variant were qualitatively the same to the ones presented so far.

Sheng and Derome (1993) have also used a vector representation of the covariances and lags between the various terms. It is noted that in their Fig. 6 the relative angles between the vectors are determined by, and interpreted as, time lags. In accord with our results, they display the advection forcing to covary and project the most on the tendency.

In the next section we examine the PV budget for the NAO during a persistent anomalous circulation (winter 1963). For that period the diagnosed budget is found to be significantly—yet not fundamentally—different from the ones presented in this section.

6. The NAO budget during blocking

Atmospheric blocking can be defined as the obstruction of the normal west to east progress of migratory cyclones and anticyclones (e.g., Geer 1996; James 1994). A blocking situation is attended by pronounced meridional flow in the upper levels, often comprising one or more closed anticyclonic (cyclonic) circulation patterns at high (low) latitudes. This anomalous circulation pattern typically remains nearly stationary or moves slowly westward and may persist for prolonged periods of typically 7–10 days or, less often, up to a month and longer. Blocking episodes have a pronounced effect on weather patterns since they are accompanied by anomalous storm activity and meridional temperature advection, as well as by large-scale subsidence in the blocking anticyclone. The occurrence and dynamics of blocking flows have been studied extensively in the past by theorists and synopticians trying to understand and predict their evolution (e.g., Benzi et al. 1986).

It is known that North Atlantic blocking correlates positively with the NAO negative phase, as shown for example in Shabbar et al. (2001). More recently, Woollings et al. (2008) have proposed a direct dynamical relationship between Rossby wave breaking and the NAO, while at the same time they point to the identity between wave-breaking events and blocking episodes.

In this section we examine the PV budget in relation to North Atlantic blocking in two different ways. First, using the discrete wave-breaking index (WB) calculated by Woollings et al. (2008), we separate the days in our dataset when this index indicates the occurrence of North Atlantic wave breaking (WB = 1) or the absence of it (WB = 0) and perform the previously described budget analysis separately for each of the two subsets.² In brief,

the aforementioned index signifies the reversal of the meridional θ gradient at the tropopause (PVU = 2 surface) occurring over some spatial and temporal thresholds, and it has also been referred to as the “blocking index,” for example in Pelly and Hoskins (2003). As used here, the index signifies such a reversal in the area 50°–60°N, 30°–70°W (south of Greenland), where the wave-breaking frequency shows the largest dependence on the NAO.

The PV budget analysis for the days of blocking (WB = 1) and nonblocking (WB = 0) in the North Atlantic showed that in both cases the balances (not shown) are nearly the same with the general DJFM budget presented in section 4. As discussed below, with the majority of the blocking events lasting 5–10 days the associated anomalies can only marginally be characterized as low-frequency occurrences. The slow PV tendency (periods of 10 days and longer) remains significant during these events, and the dominant part of the associated variability is related to propagating Rossby waves rather than to any persistent features. Lindzen (1986) discusses the concept of persistence in relation to Rossby waves and blocking, pointing out that, when referring to low-frequency variability, the concept of persistence has to indicate very long-lasting anomalies that are not the norm but the exception in the midlatitude circulation. Hence, finding that the advection forcing balances the tendency is not so surprising given that such a balance is typical for propagating waves.

To examine the PV budget for a very long lasting anomaly, we have chosen to look as well at the infamous 1963 winter. Then, an anomalously prolonged blocking episode occurred with significant departures from the climatological flow that persisted for over two months. In the North Atlantic these departures were very much like a negative NAO phase, as can be seen in a case study by O'Connor (1963).

The previously mentioned wave-breaking index for the North Atlantic sector was found to be positive throughout the period from 11 January to 18 March 1963 with the exception of four days with WB = 0 scattered through the 67-day period. The PV budget for this period is shown in Fig. 7 and there are some differences from the previously discussed cases. For the individual blocking period, the fields of the variances and covariances are less smooth since there is no time averaging over many seasons to smoothen the distributions. Also, during the persistent blocking, the variance of low frequency is found to be smaller than normal near the center of the corresponding anomalies (O'Connor 1963), while at other locations (such as upstream west of Greenland) it is larger than normal (cf. Figs. 3–7). The latter is neither unexpected nor hard to understand, especially if one considers that transients get deflected

² Variances and covariances are still meaningful for fragmented time series. For convenience, the values in the time series corresponding to the not-examined days are simply set to “missing values” and are ignored in the calculations.

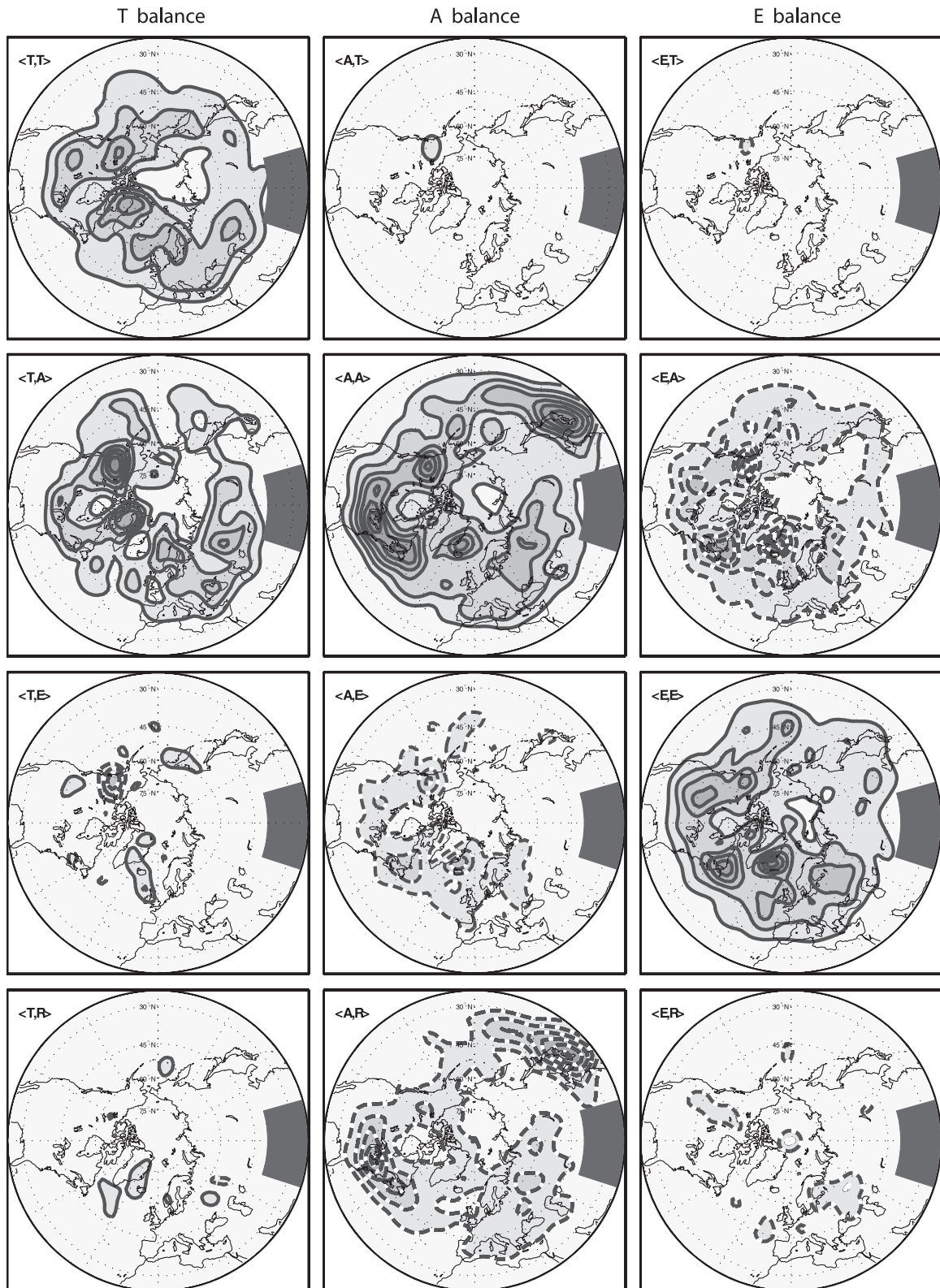


FIG. 7. As in Fig. 3 but for the examined period of persistent blocking (see text): contour interval (left to right) 0.05, 0.25, and 0.15.

meridionally upstream of the blocking and, also, it is the fastest transients (near the cutoff frequency) and not the month-to-month variations that dominate the tendency variance. As discussed previously, this dominance is due to the fact that for each Fourier component in PV variability the variance of the corresponding tendency is quadratic to the Fourier frequency. On the other hand, the balances in the PV budget during the persistent blocking are found to be basically the same as for the general case, indicating that we are looking at transient features superimposed to the slowly changing anomalies associated with the blocking.

Projecting the fields of \mathbb{T} , \mathbb{A} , and \mathbb{E} for this blocking period onto the NAO pattern and taking the covariances between the resulting time series reveals a slightly different balance for the evolution of the slowly varying NAO anomalies. By using the PV tendency instead of the PV anomalies themselves, our analysis aims to explain the evolution rather than the maintenance of the associated anomalies. In other words, when taking covariances with the tendency the transition periods count more. As in the previous section, a vector diagram (Fig. 8) is used to illustrate the balance between the time series. In this, it is seen that during the examined blocking period the PV tendency \mathbb{T} is balanced almost equally by advection \mathbb{A} and eddy forcing \mathbb{E} .

7. Findings summary and conclusions

A new approach is used for analyzing the balance between covarying terms, here applied to potential vorticity variability. Our aim is to assess the role of nonlinear synoptic eddy fluxes in driving low-frequency anomalies, as well as to understand the isentropic PV budget in general. The budget analysis [Eqs. (2)–(5)] relates the low-frequency PV tendency to the high-frequency eddy fluxes, the advection by the low-frequency component of the flow, and a term representing nonconservative effects that is calculated as a residual. A cutoff frequency separates the high-frequency and the low-frequency transients. The main findings of the point-to-point analysis are summarized as follows:

- The low-frequency PV tendency variability is largely balanced by the advection forcing, indicating that the latter forces the evolution of the associated PV anomalies.
- The eddy forcing exhibits strong variability, but it projects weakly on the slow PV tendency. Instead, its variability is mostly counterbalanced by advection.

Then, projections of the PV balance terms onto particular spatial patterns allowed for isolating the variability associated with these patterns from the bulk of low-

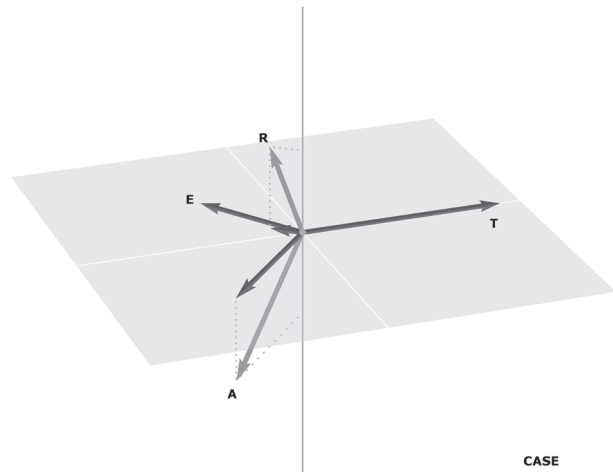


FIG. 8. As in Fig. 5 but for the NAO during the examined persistent blocking (see text).

frequency variability. The role of the various forcings was then examined—as in the previously employed PV budget analysis—for driving the variability of the patterns. For this the variances and covariances between the four terms (tendency, advection, eddy forcing, and residual) were taken, and their variability balance was illustrated with a novel vector representation. Also, particularly for the NAO, the temporal aspect of the PV budget was examined using lag composites and cross-covariances. Finally, the PV budget during a persistent blocking episode in the North Atlantic was examined when outstanding negative NAO anomalies persisted. The main findings are as follows:

- Slow advection is the leading contribution to the PV tendencies associated with the NAO, the PNA variability.
- The synoptic eddy forcing contributes about 10%–20% to the aforementioned PV tendencies. As shown with the vector diagrams, the eddy forcing is strong but projects relatively weakly onto the pattern PV tendency. The eddy forcing is largely offset by the advection.
- With respect to the NAO life cycle, the tendency is largely balanced by the advection forcing at all lags. The eddy forcing is mostly in phase with the tendency (leading the latter by about a day) and thus helps the evolution of the NAO. However, in contrast to what other studies have found (e.g., Feldstein 2003), in our analysis the eddy forcing changes sign during the NAO life cycle.
- During periods of prolonged strong NAO anomalies, the PV budget may be considerably different, with the eddy forcing balancing the tendency variability as much as the advection. The results for the case study of the 1963 winter indicate that synoptic eddy forcing

is important for the evolution of blocking episodes and, arguably, for the transition between different flow regimes.

- In the general case (for all patterns examined and for a cutoff period of 10 days), the close balance between advection and the tendency is consistent with the propagation of Rossby waves. Although periods near the cutoff are expected to dominate the tendency, other slower components in the low-frequency band also project onto the patterns.
- Finally, considering the vector balances presented, it is seen that for the NAO the eddy forcing (**E**) is less orthogonal to the tendency (**T**) compared to the corresponding vector for the PNA, and this difference is found to be accentuated during the examined case blocking. Therefore, in contrast to the PNA, which can be thought of as fitting better the Simmons et al. (1983) paradigm, part of the NAO variability can be attributed to the wave-breaking mechanism.

For studying the role of the various forcings, the approach followed is not free of drawbacks. First, it is the unclear interpretation of the strongly varying residual, which, however, does not project on the tendency. Also, one has to bear in mind that the PV budget on any isentropic surface is inseparable of, and depends on, what is happening at other levels and at the surface since the inversion operator that yields the flow field is an integral over space. Computational errors related to applying the Fourier transform to the aperiodic seasonal time series have been tested and found to be small. Also, potential errors in computing eddy PV fluxes that may arise from estimating spatial derivatives using discrete fields have been reduced using the previously described scale-selective filter. Notably, the isentropic PV distribution (instantaneous and time average) is characterized by strong localized gradients. These gradients appear to dominate both of the advective³ terms, **A** and **E**, as their variability maxima coincide with the maxima of the time-mean PV gradient. Any missed contributions from subsynoptic eddy fluxes (if significant) are part of the residual term.

Although our analysis does not dismiss the significance of the eddy forcing, it demonstrates that, as far as the PV pattern anomalies are concerned, the eddy forcing may partly induce these anomalies but its role is not dominant or sufficient by itself. Thus, our findings do not clearly support the wave breaking suggested by Benedict et al. (2004) as the primary dynamical mechanism for the NAO. Further study is needed to feel the gap.

³ The **A** term is called advective in the sense that is a product of a velocity times a gradient.

As shown in our analysis of the PV budget during a persistent blocking, the above-discussed balances may vary in periods when there are long-lasting NAO anomalies. However, such periods represent a small fraction of time in NAO variability. Following from our results, the PV variability associated with the NAO teleconnection appears to consist largely of propagating Rossby waves. This can be possibly understood in the spirit of the Simmons et al. (1983) study where extratropical low-frequency patterns were produced in response to remote forcings. On the other hand, Woollings et al. (2008) see the NAO variability as the transition between blocking events and the regular westerly flow over the North Atlantic. Our results suggest that the eddy forcing is partly responsible for these transitions, but advection remains equally important for balancing the PV tendency.

Acknowledgments. The authors are grateful to the Joint Institute for the Study of the Atmosphere and Ocean (JISAO) for covering the publishing charges. We thank Brian Hoskins for insightful discussions during the course of this work, as well as Paul Berrisford and Mark Baldwin for their help in obtaining the ERA-40 isentropic potential vorticity data. This publication is funded under NOAA Cooperative Agreement NA17RJ1232.

REFERENCES

- Athanasiadis, P. J., and M. H. P. Ambaum, 2009: Linear contributions of different time scales to teleconnectivity. *J. Climate*, **22**, 3720–3728.
- Benedict, J. J., S. Lee, and S. B. Feldstein, 2004: Synoptic view of the North Atlantic Oscillation. *J. Atmos. Sci.*, **61**, 121–144.
- Benzi, R. B. Saltzman, and A. Wiin-Nielsen, Eds., 1986: *Anomalous Atmospheric Flows and Blocking*. *Advances in Geophysics*, Vol. 29, Academic Press, 459 pp.
- Branstator, G. W., 1992: The maintenance of low-frequency atmospheric anomalies. *J. Atmos. Sci.*, **49**, 1924–1945.
- Brunet, G., R. Vautard, B. Legras, and S. Edouard, 1995: Potential vorticity on isentropic surfaces: Climatology and diagnostics. *Mon. Wea. Rev.*, **123**, 1037–1058.
- Cai, M., and H. M. Van Den Dool, 1994: Dynamical decomposition of low-frequency tendencies. *J. Atmos. Sci.*, **51**, 2086–2100.
- Derome, J., G. Brunet, and Y. Wang, 2001: On the potential vorticity balance on an isentropic surface during normal and anomalous winters. *Mon. Wea. Rev.*, **129**, 1208–1220.
- Edouard, S., R. Vautard, and G. Brunet, 1997: On the maintenance of potential vorticity in isentropic coordinates. *Quart. J. Roy. Meteor. Soc.*, **123**, 2069–2094.
- Feldstein, S. B., 2003: The dynamics of NAO teleconnection pattern growth and decay. *Quart. J. Roy. Meteor. Soc.*, **129**, 901–924.
- , and S. Lee, 1998: Is the atmospheric zonal index driven by an eddy feedback? *J. Atmos. Sci.*, **55**, 3077–3086.
- Geer, I. W., 1996: *Glossary of Weather and Climate*. Amer. Meteor. Soc., 272 pp.

- Hartmann, D. L., and F. Lo, 1998: Wave-driven zonal flow vacillation in the Southern Hemisphere. *J. Atmos. Sci.*, **55**, 1303–1315.
- Hoerling, M. P., 1992: Diabatic sources of potential vorticity in the general circulation. *J. Atmos. Sci.*, **49**, 2282–2292.
- Holton, J. R., 2004: *An Introduction to Dynamic Meteorology*. 4th ed. Int. Geophysics Series, Vol. 88, Academic Press, 535 pp.
- James, I. N., 1994: *Introduction to Circulating Atmospheres*. Cambridge Atmospheric and Space Science Series, Cambridge University Press, 422 pp.
- Kállberg, P., P. Berrisford, B. J. Hoskins, A. Simmons, S. Uppala, and S. Lamy-Thépaut, 2005: *ERA-40 Atlas*. ERA-40 Project Report Series, Vol. 19, ECMWF, 82–85.
- Limpasuvan, V., and D. L. Hartmann, 2000: Wave-maintained annular modes of climate variability. *J. Climate*, **13**, 4414–4429.
- Lindzen, R. S., 1986: Stationary planetary waves, blocking and interannual variability. *Advances in Geophysics*, Vol. 29, Academic Press, 251–273.
- Lorenz, D. J., and D. L. Hartmann, 2003: Eddy–zonal flow feedback in the Northern Hemisphere winter. *J. Climate*, **16**, 1212–1227.
- Massacand, A. C., and H. C. Davies, 2001: Interannual variability of European winter weather: The potential vorticity insight. *Atmos. Sci. Lett.*, **2**, 52–60.
- O'Connor, J. F., 1963: The weather and circulation of January 1963. *Mon. Wea. Rev.*, **91**, 209–218.
- Pelly, J. L., and B. J. Hoskins, 2003: A new perspective on blocking. *J. Atmos. Sci.*, **60**, 743–755.
- Robinson, W. A., 1996: Does eddy feedback sustain variability in the zonal index? *J. Atmos. Sci.*, **53**, 3556–3569.
- , 2000: A baroclinic mechanism for the eddy feedback on the zonal index. *J. Atmos. Sci.*, **57**, 415–422.
- Sardeshmukh, P. D., and B. J. Hoskins, 1984: Spatial smoothing on the sphere. *Mon. Wea. Rev.*, **112**, 2524–2529.
- Shabbar, A., J. Huang, and K. Higuchi, 2001: The relationship between the wintertime North Atlantic Oscillation and blocking episodes in the North Atlantic. *Int. J. Climatol.*, **21**, 355–369.
- Sheng, J., and J. Derome, 1993: Dynamical forcing of the slow transients by synoptic-scale eddies: An observational study. *J. Atmos. Sci.*, **50**, 757–771.
- Simmons, A. J., J. M. Wallace, and G. W. Branstator, 1983: Barotropic wave propagation and instability, and atmospheric teleconnection patterns. *J. Atmos. Sci.*, **40**, 1363–1392.
- Swanson, K. L., 2001: Upper-tropospheric potential vorticity fluctuations and the dynamical relevance of the time mean. *J. Atmos. Sci.*, **58**, 1815–1826.
- , 2002: Dynamical aspects of extratropical tropospheric low-frequency variability. *J. Climate*, **15**, 2145–2162.
- Tyrlis, V., and B. J. Hoskins, 2008: Aspects of a Northern Hemisphere atmospheric blocking climatology. *J. Atmos. Sci.*, **65**, 1638–1652.
- Uppala, S. M., and Coauthors, 2005: The ERA-40 re-analysis. *Quart. J. Roy. Meteor. Soc.*, **131**, 2961–3012.
- Valdes, P. J., and B. J. Hoskins, 1989: Linear stationary wave simulations of the time-mean climatological flow. *J. Atmos. Sci.*, **46**, 2509–2527.
- Vallis, G. K., E. P. Gerber, P. J. Kushner, and B. A. Cash, 2004: A mechanism and simple dynamical model of the North Atlantic Oscillation and annular modes. *J. Atmos. Sci.*, **61**, 264–280.
- Von Storch, H., and F. W. Zwiers, 1999: *Statistical Analysis in Climate Research*. Cambridge University Press, 484 pp.
- Woollings, T., B. J. Hoskins, M. Blackburn, and P. Berrisford, 2008: A new Rossby wave-breaking interpretation of the North Atlantic Oscillation. *J. Atmos. Sci.*, **65**, 609–626.